Fragility Function Development and Seismic Loss Assessment of Expansion Joints

Otsuki, Yu; Kurata, Masahiro; Skalomenos, Konstantinos; Ikeda, Yoshiki; Akazawa, Motoki

FRAGILITY FUNCTION DEVELOPMENT AND SEISMIC LOSS ASSESSMENT OF EXPANSION JOINTS

Yu Otsuki[1], Masahiro Kurata[2], Konstantinos A. Skalomenos[2], Yoshiki Ikeda[2], and Motoki Akazawa[3]

[1]Graduate School of Engineering, Kyoto University, Kyoto-shi, Kyoto, 615-8530, Japan,
otsuki.yu.65n@st.kyoto-u.ac.jp, corresponding author
[2]Disaster Prevention Research Institute, Kyoto University
[3]Structural Engineering Section, Takenaka Corporation

Expansion joints are used as a special connection equipment between adjacent buildings to accommodate the relative motions generated by wind, thermal, or earthquake loads, but they often exhibit damage during severe earthquakes. The level of damage and safety factors required to avoid loss of function are not well considered in current design practices. The objective of this paper is to provide quantitative information on the seismic damage probability of common expansion joints and the associated repair costs. The designer and engineer can refer to this information as a basis for decision-making in the selection of expansion joints. Four common types of expansion joints are considered: high- and standard-performance floor and wall expansion joints, whose damage states have been evaluated recently by the authors through shaking table tests. First, the fragility functions of expansion joints for seven damage patterns are developed utilizing the test results. Next, the vulnerability of expansion joints installed between adjacent building models is assessed via incremental dynamic analysis. The recommended level of safety factor to ensure the function of expansion joints is discussed. Finally, a procedure for cost-effective selection of expansion joints is introduced, where case studies are examined using buildings with different characteristics. The presented results are deemed to be beneficial for improving the design practice of expansion joints and for reducing future seismic loss.

KEYWORDS

Expansion joints, non-structural components, fragility function, relative displacement, adjacent buildings.

1 INTRODUCTION

Decisions regarding the design of buildings in seismic regions are often made in terms of the seismic risk expected within the lifespan of the building. Damage of non-structural components caused by earthquakes results in significant economic loss, which sometimes can exceed the replacement cost of the entire building [Sullivan *et al*. 2018]. Non-structural damage also causes serious injuries and economic loss, but current seismic design methodologies consider non-structural damages indirectly by checking drift limits and floor acceleration [Nakashima et al. 2018, Lee et al. 2007, Anajafi and Medina 2018]. For risk assessment, the fragility functions of various building components [Skalomenos et al. 2015, Sarno et al. 2019, Porter 2016, Pardalopoulos and Pantazopoulou 2015, Konstantinidis and Markris 2009] and associated information on repair cost, procedure, and time are necessary [Porter 2003]. The Federal Emergency Management Agency (FEMA) provides relevant information for a wide variety of structural and non-structural components, and the Applied Technology Council (ATC) recently developed an electronic Performance Assessment Calculation Tool (PACT) to perform probabilistic computations and accumulation of losses [FEMA 2012].

Expansion joints are used as a special connection equipment between adjacent buildings to accommodate the relative motions generated by wind, thermal, or earthquake loads, but they often exhibit damage during severe earthquakes. However, the damage limit states of expansion joints and the safety factors required to avoid failure are not well considered in current design practice. In addition, fragility information for expansion joints has not yet been prepared and the vulnerability and seismic loss analyses of expansion joints are not available. Expansion joints on apartment buildings dropped off during the 2005 Fukuoka earthquake [AIJ 2005] and the 2016 Kumamoto earthquake [NILIM and BRI 2016], while 90 of 327 expansion joints on base-isolated buildings were heavily damaged during the 2011 Tohoku earthquake [Kasai *et al*. 2013]. Seismic poundings between adjacent buildings were observed in past earthquakes, which could result in a significant damage to expansion joints [Bertero *et al*. 1986, Filiatrault *et al*. 1994, Kasai *et al*. 1997, PWRI 1997, and Cole *et al*. 2012]. Especially after the 2011 Tohoku earthquake, owners and researchers are putting more emphasis on the seismic performance of non-structural components, owing to their impacts on building serviceability and risk management [AIJ 2013, Nakashima et al. 2018, Isobe et al. 2018]. In keeping with these campaigns, guidelines for expansion joints were recently published by the Japanese Society of Seismic Isolation (JSSI) [2013] and the Japan Expansion Joint Association (JEJA) [2016], an association consisting of six expansion joint manufacturers. These guidelines discuss the basic behavior, damage states, and testing of expansion joints within the design range of motion, but the performance of expansion joints beyond the design range of motion is not well addressed.

The typical seismic design of expansion joints used in adjacent buildings is illustrated in Figure 1(a), where the key design parameters are i) the minimum separation distance between the buildings, ii) the safety factor, and iii) the nominal range of motion of expansion joints. Figure 1(b) illustrates the definitions of each parameter for a typical floor expansion joint. Seismic codes prescribe a minimum separation distance between two buildings for avoiding seismic pounding and provide simplified methods for estimating the peak relative displacement [BCJ 2008, ICBO 1997, CEN 2005, and TBC 1997]. In a performance-based design framework, a probabilistic analysis procedure for estimating the seismic pounding risk was recently developed [Tubaldi 2016]. A safety factor is selected by structural engineers to determine the clearance between the adjacent buildings; the clearance is calculated as the product of the minimum separation distance and the safety factor. The value of the safety factor is determined based on the experience of engineers , owing to the lack of a quantitative relation between the safety factor and element performance. The design range of motion of expansion joints, defined as the ratio of the clearance distance between two buildings, typically ranges from 20% to 80% [JEJA 2016]. When this ratio is smaller than the reciprocal of the safety factor, there is a possibility of damage to the expansion joints, even under code-level ground motions. As pointed out by Kasai *et al*. [2013], one of the major source of damage to expansion joints in the 2011 Tohoku earthquake was the insufficient range of motion. Therefore, a quantitative evaluation of safety factors and damage to expansion joints is necessary to provide a basis for decision makers in the design process.

Regarding the seismic capacity of expansion joints, there are several performance levels used in Japan. The JSSI [2013] defines three seismic performance ranks for expansion joints in base-isolated buildings, namely the A, B, and C rank. The JEJA [2016] issued a guideline that explains the basic behavior and damage states of expansion joints for general buildings, referring to the desirable performance of expansion joints as recommendations for seismic design and construction of non-structural components [AIJ 2003]. To investigate the different seismic performance and damage pattern of various expansion joints, the authors have conducted shaking table tests for four commonly used types: high-performance (HP) and standard-performance (SD) floor and wall expansion joints. In total, seven damage patterns were observed. As expected, the HP expansion joints showed better seismic performance than the SD expansion joints that failed immediately after reaching the predefined nominal range of motion [Otsuki *et al*. 2018a]. These results suggest that the safety factor considered in the design process should be different for reaching various levels of performance in expansion joints.

The objective of this paper is to evaluate the vulnerability and seismic loss of expansion joints for different seismic performance levels and safety factors. First, fragility functions of expansion joints are developed by using the available test data. Then, vulnerability and seismic loss analysis are conducted using two sets of adjacent building models. Using the results of incremental dynamic analyses and the developed fragility functions, the relationship between safety factor and damage probability of expansion joints is investigated. The presented results offer structural designers and building owners with a basis for quantitative decision-making in the selection of expansion joints.

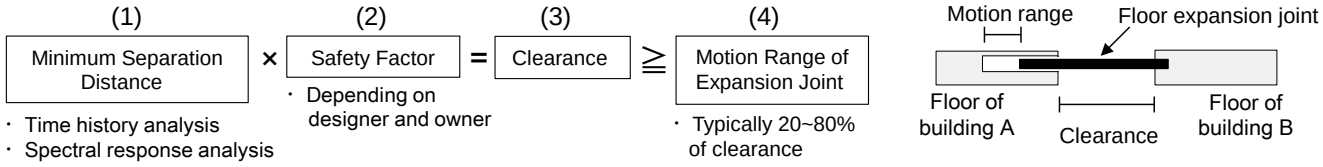

Figure 1 Overview of expansion joints: (a) Seismic design of expansion joints and (b) definition of clearance and range of motion for a typical floor expansion joint.

2 DAMAGE PATTERNS OF EXPANSION JOINTS OBSERVED IN SHAKING TABLE TESTS

This section provides with an overview of the behavior and damage states of expansion joints as observed in shaking table tests conducted by the authors. The detail explanation of each mechanism and additional figures can be found in [Otsuki *et al*. 2018a]. Table 1 summarizes the deformation mechanisms, drawings, and damage states of the expansion joints. Some of the damage patterns are presented in Figure 2. The high-performance (HP) expansion joints are designed for base-isolated buildings and conformed to rank A [JSSI 2013]. These types were custom-made. The standard-performance (SD) expansion joints are widely used for general buildings and were off-the-shelf. The expansion joints were set between two steel frames with fundamental periods of 6.0 s and 0.46 sec., respectively. A sequential damage to the expansion joints was imposed using sine waves of 1 Hz with amplitudes ranging from 3.0 m/s^2 to 6.0 m/s^2 along the X-direction. The nominal range of motion of the expansion joints in the X direction was 175 mm, which corresponds to 50% of the clearance. Note that the nominal range of motion set by the manufacturer is different from the median capacity of the expansion joints. This is because each manufacturer assumes a certain extent of safety margin beyond the nominal range of motion. The damage observed in the tests were classified by using the definition by JSSI, i.e. Serviceable, Damage State 1 (DS1) for minor damage, DS2 for severe damage, and Failure for the loss of functionality [JSSI 2013]. These are sequential damage, which means a component must enter DS1 before DS2 or Failure. For minor damage, which took place simultaneously, DS-1A and DS-1B were defined as simultaneous damage. With simultaneous damage, a damaged component can be in more than

one damage state at the same time [Porter et al 2007]. In the tests, seven damage patterns were observed and the critical relative displacement that initiates each damage state was presented.

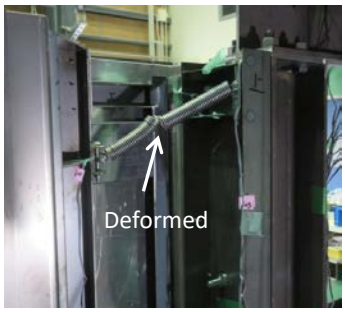

(a)

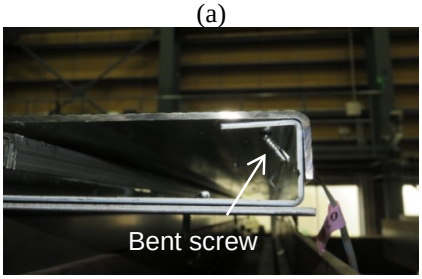

(b)

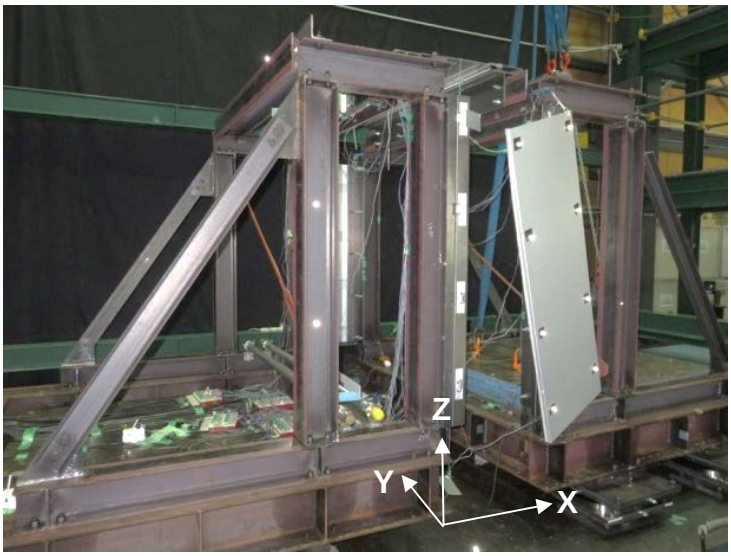

(c)

Figure 2 Some of the damage to expansion joints observed in shaking table tests [Otsuki *et al*. 2018a]: (a) HP wall DS1-A (spring deformation), (b) SD floor DS1 (screw rupture), (c) SD wall Failure (cover plate dropped off).

2.1 HP floor expansion joint

The deformation mechanism of the HP floor expansion joint is categorized as a sliding type. Most of the parts of the expansion joint were made of steel. The cover plate was not fixed in the Z-direction in Table 1, thus permitting vertical deformation. This expansion joint has a re-centering mechanism to pull back the cover plate to the initial position after an excitation and eliminate residual displacement.

As DS1, the disengagement of the cover plate due to collision between the two frames was considered. This damage can be easily fixed by relocating the cover plate to the original position. The critical relative displacement was nearly 200% of the nominal range of motion of 175 mm, demonstrating its high deformation capacity.

2.2 HP wall expansion joint

The HP wall expansion joint is categorized as a lifting type. The cover plate was lifted when the expansion joint was subjected to displacement in the Y-direction or compressive displacement in the X-direction in Table 1, but the springs pulled back the cover plate to the original position after an excitation. This expansion joint was also made of steel.

Two damage states, DS1-A and DS1-B were identified for the HP wall expansion joint. The DS1-A refers to the damage of springs as shown in Figure 2(a). Three of five springs inside the cover plate were caught on a surrounding member at the time of compression, and a permanent deformation remained in the spring. The DS1-B refers to the rupture of screws in the base material, due to the impact force applied at the time of the collision. The critical relative displacements of both damage patterns were respectively nearly equal to 110% and 130% of the nominal range of motion. These damage patterns occurred nearly at the same time as indicated by the critical relative displacement values in Table 1, and thus were categorized into simultaneous damage state.

2.3 SD floor expansion joint

The deformation mechanism of the SD floor expansion joint is categorized as a sliding type. This expansion joint consisted of an unfixed center cover plate with side plates made of stainless steel. Rubber sheets were fixed in between the cover plate and side plates. A total of twenty drill screws in the side plates were used. This expansion joint exhibited a residual displacement after an excitation because there was no re-center mechanism to pull back the cover plate to the initial position.

The rupture of the screws shown in Figure 2(b) was considered as DS1. When the two frames approached, the cover plate attached the screws several times, imposing large bending deformations which triggered the failure of screws. Then, when a large relative displacement was applied, the cover plate was disengaged from the side plate. The cover plate could no longer sustain human weight and the functionality of expansion joint was lost. This damage was classified as Failure.

The DS1 was identified within the range of motion and the Failure occurred at approximately 130% of the nominal range of motion. These are sequential damage because the cover plate must damage the side screws before the Failure occurs.

2.4 SD wall expansion joint

The deformation mechanism of the SD wall expansion joint is categorized as a rail-sliding type. The cover plate was equipped with four sliders that permitted deformation in the X-direction. The length of the slider was 175 mm. All plates and sliders were made of aluminum. The rubber sheets were equipped between the cover plate and surrounding materials.

DS1 was defined as the disengagement of the rubber sheets due to rubbing with the surrounding components. This damage led to concerns about air and water leakage. This damage resulted from the repeated loading during shakings, and therefore it is difficult to identify the critical demand value that initiates the damage. When relative displacement reached just beyond the nominal range of motion, the cover plate dropped off because its sliders went off the rails (Figure 2(c)). This damage was classified as Failure because the functionality of the expansion joint was lost. Since DS1 was observed several times before the Failure, these two damage states were considered sequential.

3 DEVELOPMENT OF FRAGILITY FUNCTIONS FOR EXPANSION JOINTS

3.1 Fragility functions for displacement-dependent damage

This section develops fragility functions of the expansion joints in component level using the test results. A fragility function expresses the probability of being in or exceeding a damage state (*DS*) as a function of an engineering demand parameter (*EDP*). The cumulative lognormal distribution is typically used to define a fragility function [Porter *et al*. 2007]. The fragility function is expressed in the form:

$$P[DS \geq ds_i \mid EDP = edp] = \Phi\left(\frac{\ln edp - \ln \theta_{c,i}}{\beta_{c,i}}\right), \tag{1}$$

where $\Phi()$ is the standard normal cumulative distribution function and $\theta_{c,i}$ and $\beta_{c,i}$ are the median and standard deviation of the natural logarithm of the capacity to resist damage state ds_i. For sequential damages, the probability of being in a specified damage state $DS = ds_i$ given a particular value of $EDP = edp$ is expressed by:

$$P(ds_i \mid edp) = \begin{cases} P[DS \geq ds_i \mid edp] - P[DS \geq ds_{i+1} \mid edp] & 1 \leq i < n \\ P[DS \geq ds_i \mid edp] & i = n \end{cases}, \tag{2}$$

where $n = 2$ in this study with ds_1 = DS1 and ds_2 = Failure.

To develop fragility functions, various methods have been proposed. Especially for displacement-sensitive damage, *i.e.*, the case of expansion joints, FEMA recommends the following methodology to develop fragility functions: “The median displacement demand at initiation of Failure should be taken as the calculated available length of travel based on the specified travel allowance dimension. The dispersion should be estimated based on the likelihood that the initial position of the structure is out of tolerance. Normal construction tolerances can be considered as representing one standard deviation on the displacement dimension. The dispersion can then be taken as equal to the coefficient of variation, which is approximated by the standard deviation value (*i.e.*, construction tolerance), divided by the median (*i.e.*, travel allowance dimension)” [FEMA 2012]. Considering the above descriptions and the available test data, the procedure for developing fragility functions of expansion joints is summarized as follows:

- Define the median $\theta_{c,i}$ using a critical length specified from the design drawings or a critical measurement value obtained by the experiment.
- Define the dispersion $\beta_{c,i}$ dividing the initial position errors expected in expansion joints by the travel allowance dimension if it is totally displacement sensitive damage or else follow the value recommended by FEMA [2012].

3.2 Initial position errors of expansion joints

The initial positions of expansion joints may contain four inherent errors: construction error, dry expansion and contraction, heat expansion and contraction, and residual displacement. The expected maximum values for each error in the positions of expansion joints for base-isolated buildings are provided by JSSI [2010] and are listed in Table 2. Because these values are for expansion joints of base-isolated buildings, a proper modification is required when they are applied for the current SD expansion joints, which are not commonly used for base-isolated buildings. The difference expected in the deformation mechanisms between expansion joints used in isolated buildings and those used in common buildings is related to the residual displacement. The expected residual displacement of the SD expansion joints was more than 10 mm, based on observations by the authors during the tests, or 30 mm based on engineering judgment.

The probability distribution of each error was assumed to follow a normal distribution with zero mean value and the maximum errors shown in Table 2 as three standard deviations. Thus, the total standard deviation for the HP expansion joints, denoted by σ_{HP}, was calculated as 8.3 mm and that for the SD expansion joints, denoted by σ_{SD}, was 126 mm.

Table 1 Summary of tested expansion joints and damage states [Otsuki *et al*. 2018a]

	High-performance floor expansion joint	**High-performance wall expansion joint**		**Standard-performance floor expansion joint**		**Standard-performance wall expansion joint**	
Deformation mechanism	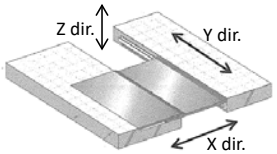 Sliding type	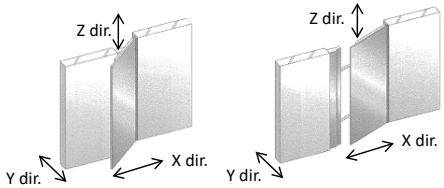 Lifting type		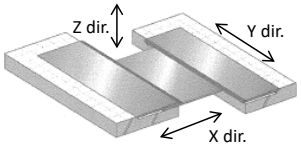 Sliding type		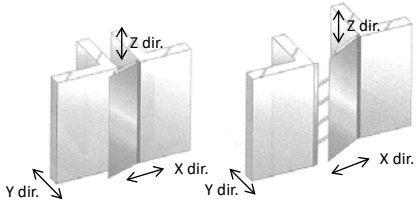 Sliding type	
Drawing	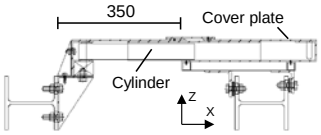	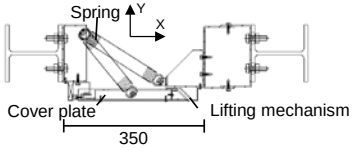		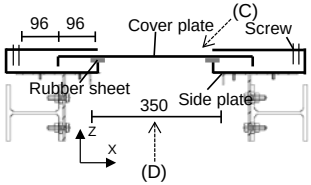		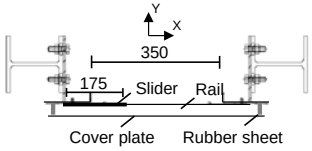	
Damage state	DS1 Cove Plate Disengaged	DS1-A Spring Deformation	DS1-B Screw Rupture	DS1 Screw Rupture	Failure Cover Plate Disengaged	DS1 Rubber Sheet Disengaged	Failure Cover Plate Dropped Off
Damage description	Cover plate was disengaged, due to collisions with other components. Cover plate can be easily fixed by relocating it to the original position.	Three of five springs had residual deformations after collisions with other components.	Screws were fractured, due to the impact force applied when collisions occurred.	Drill screws were bent and ruptured, due to several collisions with the cover plate.	Cover plate was disengaged from the side plate, creating a gap between floors.	Rubber sheets were disengaged, creating a gap that led to concerns about air and water leakage.	Cover plate fell off because its sliders went off the rails.
Critical relative displacement (ratio to the range of motion of 175 mm)	338 mm (193%)	191 mm for one spring and 236 mm for the other two springs (109% and 132%)	203 mm (116%)	94 mm (54%)	222 mm (127%)	– (Due to rubbing with other components)	176 mm for the front wall and 190 mm for the back wall (101% and 109%)

Table 2 Initial position errors expected in expansion joints (unit: mm) [JSSI 2010].

	HP expansion joints	SD expansion joints
Construction	±20	±20
Dry expansion and contraction	±10	±10
Heat expansion and contraction	±5	±5
Residual displacement	±10	±30
Total standard deviation by assuming 3σ = sum of the above maximum values	$\sigma_{HP} = \sqrt{\left(\frac{20}{3}\right)^2 + \left(\frac{10}{3}\right)^2 + \left(\frac{5}{3}\right)^2 + \left(\frac{10}{3}\right)^2}$ = 8.3	$\sigma_{SD} = \sqrt{\left(\frac{20}{3}\right)^2 + \left(\frac{10}{3}\right)^2 + \left(\frac{5}{3}\right)^2 + \left(\frac{30}{3}\right)^2}$ = 12.6

3.3 Fragility functions for expansion joints

Table 3 presents the fragility functions of each expansion joint. The horizontal axis represents the normalized relative displacement defined as the critical relative displacement over the nominal range of motion D_{expj} of 175 mm. The dashed line in each fragility function indicates the nominal range of motion. The small dots express the normalized relative displacements measured at each input. The dots at probability 0 indicate the peak normalized relative displacement measured during each input before the occurrence of damage. The dots at probability 1 indicate the normalized relative displacement at the time of damage (*i.e.*, critical relative displacement in Table 1 over the nominal range of motion) described in Otsuki *et al*. [2018a]. The details of each fragility function are explained in the following sections.

3.3.1 *HP floor expansion joint DS1: cover plate disengaged*

In the test, the cover plate of the HP expansion joint was disengaged as a result of a collision between the cover plate and side plate. The critical relative displacement for this damage was 338 mm, which was nearly equal to 200% of the nominal range of motion of 175 mm (338/175 = 1.92). Therefore, the median value of the normalized relative displacement was adopted as $\theta_{c,i}$ = 2.0 m. A large dispersion must be considered because the collision does not always occur even when the relative displacement reached 338 mm [Otsuki *et al*. 2018a]. When a fragility function incorporates such a large uncertainty, FEMA [FEMA 2012] suggests to use a dispersion of $\beta_{c,i}$ = 0.4. However, assuming $\beta_{c,i}$ = 0.4, DS1 could happen even within the nominal range of motion, as shown in Table 3, which is not consistent with the test results. Therefore, $\beta_{c,i}$ = 0.25 is adopted in the present study so that the damage probability at the design value equals zero.

3.3.2 *HP wall expansion joint DS1-A: spring deformation*

Some springs of the HP wall expansion joint experienced residual displacements after the surrounding components of expansion joint collided with the springs. Table 4 lists the maximum relative displacements on the compression side and the number of damaged springs during each input. The critical relative displacement for this damage state was uncertain [Otsuki *et al*. 2018a] and the maximum relative displacement for each input was used to calculate the median and dispersion values. Following the procedure in FEMA [2012], the median $\theta_{c,i}$ = 1.26 and the dispersion $\beta_{c,i}'$ = 0.086 were obtained. In case of five or fewer specimens, it is recommended to increase the dispersion by 0.25 [FEMA 2012]. Thus, the total dispersion $\beta_{c,i}$ was obtained as 0.265. The procedure is as follows:

$$\theta_{c,i} = \frac{\exp\left(\frac{1}{n_i}\sum_{i=1}^{n_i}\ln(r_i)\right)}{D_{\exp}} = \frac{\exp\left(\frac{\ln(191)+\ln(236)+\ln(236)}{3}\right)}{175} = \frac{220}{175} = 1.26 \tag{3}$$

$$\beta_{c,i}' = \sqrt{\frac{1}{n_i - 1}\sum_{i=1}^{n_i}\left(\ln\left(r_i / \theta_{c,i} D_{\exp}\right)\right)^2} = 0.086$$

$$\beta_{c,i} = \sqrt{0.086^2 + 0.25^2} = 0.265 \tag{4}$$

Table 4 Experimental results for damage of springs [Otsuki *et al*. 2018a].

Input amplitude of sinewave 1 Hz (m/s^2)	Maximum relative displacement on the compression side r_i (mm)	Total of damaged springs n_i of five springs
4.0	191	1
6.0	236	3

Table 3 Fragility functions of expansion joints with nominal range of motion D_{expj} of 175 mm.

HP floor expansion joint **DS1: Cover plate disengaged** $\theta_{c,i} = 2.00$ $\beta_{c,i} = 0.250$	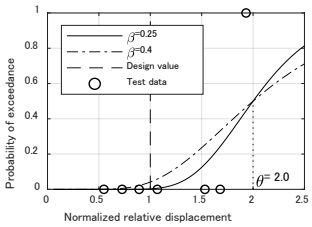	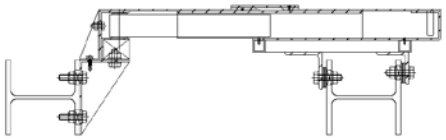
HP wall expansion joint **DS1-A: Spring deformation** $\theta_{c,i} = 220 / D_{expj} = 1.26$ $\beta_{c,i} = 0.265$	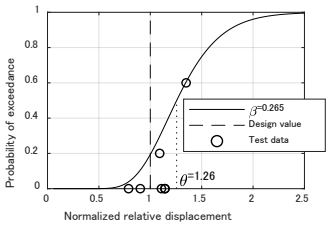	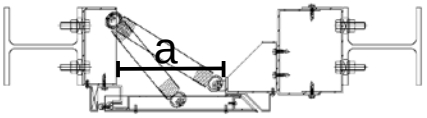
HP wall expansion joint **DS1-B: Screw rupture** $\theta_{c,i} = a/D_{expj} = 1.20$ $\beta_{c,i} = \frac{\sigma_{HP}}{\theta_{c,i} D_{expj}} = \frac{8.3}{210} = 0.040$	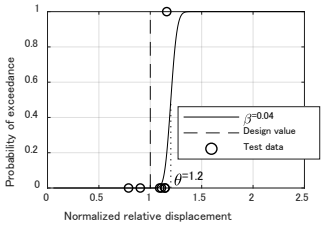	
SD floor expansion joint **DS1: Screw rupture** $\theta_{c,i} = a/D_{expj} = 0.55$ $\beta_{c,i} = 0.400$	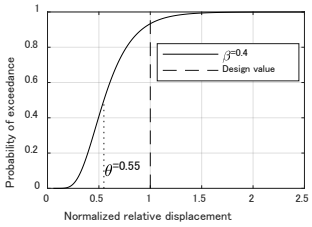	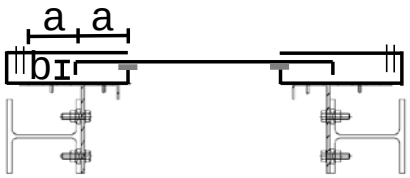
SD floor expansion joint **Failure: Cover plate disengaged** $\theta_{c,i} = 2(a+b)/D_{expj} = 1.29$ $\beta_{c,i} = \frac{\sigma_{SD}}{\theta_{c,i} D_{expj}} = \frac{12.6}{226} = 0.056$	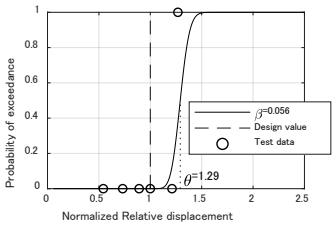	
SD wall expansion joint **DS1: Rubber sheet disengaged** $\theta_{c,i} = 0.85$ $\beta_{c,i} = 0.400$	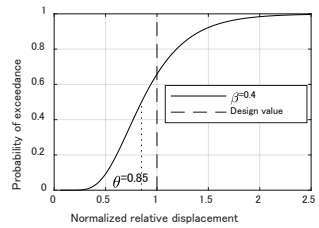	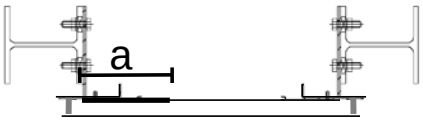
SD wall expansion joint **Failure: Cover plate dropped off** $\theta_{c,i} = a/D_{expj} = 1.00$ $\beta_{c,i} = \frac{\sigma_{SD}}{\theta_{c,i} D_{expj}} = \frac{12.6}{175} = 0.072$	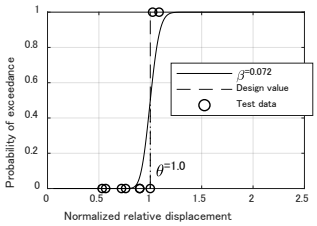	

3.3.3 *HP wall expansion joint DS1-B: screw rupture*

Several screws of the HP wall expansion joint were damaged by the large impact force imposed when the two frames repeatedly collided. Therefore, the distance between the collision points, denoted by a, is critical for this damage and the median value was set as $\theta_{c,i} = a/D_{expj} = 210/175 = 1.20$. The dispersion $\beta_{c,i} = 0.04$ was obtained by dividing the standard deviation of initial position errors, $\sigma_{HP} = 8.3$ mm, by $\theta_{c,i}\, D_{expj} = 210$ mm.

3.3.4 *SD floor expansion joint DS1: screw rupture*

The damage to the screws depends on the length of the cover plate and the screws, as indicated by a in Table 3. The test results confirmed that collision between the cover plate and screws was likely to occur when the relative displacement reached half of the expected collision distance $2a$, owing to the imbalance of the friction coefficient of the rubber sheets [Otsuki *et al*. 2018a]. Thus, the median value of this damage state was taken as $\theta_{c,i} = a/D_{expj} = 9.6/175 = 0.055$. The screws were ruptured after repeated collisions. Therefore, a large dispersion should be considered and $\beta_{c,i} = 0.4$ was adopted in this study which is proposed by FEMA [2012] for cases with large uncertainty.

3.3.5 *SD floor expansion joint failure: cover plate disengaged*

The disengagement of the cover plate of the SD floor expansion joint depends on the dimensions a and b of the cover plate in Table 3. The critical relative displacement measured in the test was 222 mm, which equaled nearly $2(a + b) = 226$ mm. Therefore, the median value was taken as $\theta_{c,i} = 226 / D_{expj} = 226 / 175 = 1.29$. The dispersion $\beta_{c,i} = 0.056$ was obtained by dividing the standard deviation of the initial position errors $\sigma_{SD} = 12.6$ mm by $\theta_{c,i} D_{expj} = 226$ mm.

3.3.6 *SD wall expansion joint DS1: rubber sheet disengaged*

The rubber sheet of the SD wall expansion joint was disengaged due to the repeated rubbing with the surrounding materials of the expansion joint during shakings. This damage state cannot be totally displacement-dependent, but is assumed here as same as the other damage states. This damage state was not observed after the input of 3.0 m/s^2 and 3.5 m/s^2, but it was observed after the input of 4.0 m/s^2. The peak relative displacements during the excitation of 3.0 m/s^2 and 3.5 m/s^2 were 153 mm and 151 mm, respectively, which equaled nearly 85% of the nominal range of motion. Thus, the median value was taken as $\theta_{c,i} = 0.85$. Considering the large uncertainty of the occurrence of this damage, $\beta_{c,i}$ was set equal to 0.40 based on the recommendation of FEMA (2012).

3.3.7 *SD wall expansion joint failure: cover plate dropped off*

The test results showed that the cover plate of the SD wall expansion joint dropped off exactly when the relative displacement exceeded the sliding length. Thus, the median value was taken as $\theta_{c,i} = a/D_{expj} = 175/175 = 1.0$. The value of dispersion $\beta_{c,i}$ was obtained equal to 0.072 by dividing the standard deviation of the initial position errors $\sigma_{SD} = 12.6$ mm by $\theta_{c,i}\, D_{expj} = 175$ mm.

4 ADJACENT BUILDING MODEL

The peak relative displacement between adjacent buildings depends on building characteristics, such as, the fundamental period, damping ratio, and the type of force–displacement hysteresis curve [Kasai 1996, Tubaldi 2015]. To examine the effect of building characteristics on the selection of expansion joints, two types of adjacent buildings were prepared, as shown in Figure 3. One adjacent building model consists of a 55-story super-high-rise building and a 13-story high-rise building. This is called the SH model (S stands for Super high-rise and H for High-rise). The other adjacent building model consists of two 13-story high-rise buildings. This is called the HH model (H stands for High-rise and High-rise). For both types of adjacent buildings, a sky bridge with the tested expansion joints is assumed at a height of 44 m. The expansion joints and sky bridge are not modelled as they slightly contribute to the dynamic response of the buildings compared to the main structural systems.

The 55-story super-high-rise building is a 238-m-high steel structure with 55 stories above (54 floors and a roof) and 6 stories below ground level. The spread foundation is secured over the bedrock layer at a depth of around 30 m underground. The first natural period is 5.79 s. The structural system of the building is a combination of steel moment-resisting frames with oil dampers and buckling-restrained braces. More detailed information and results of seismic response analysis can be found in the authors' previous work [Otsuki *et al*. 2018b]. The 13-story high-rise building is a 52-m-high steel structure with buckling-restrained braces. It has 13 stories above the ground and a story underground. The first natural period is 1.37 s. Both buildings were designed to satisfy the current Japanese building code. The SH model consists of these two buildings.

The HH model is composed of the above 13-story building (referred as original 13-story building) and an adjusted 13-story building of similar characteristics. In general, the periods of adjacent buildings with the same heights are not equal, owing to the difference on mass and stiffness either accidentally nor in purpose [Lin and Weng 2001]. Therefore, the

adjusted 13-story building was created by multiplying the mass of each floor of the original 13-story building by 1.2. The natural period of the adjusted 13-story building is 1.50 s. The locations of the buildings are assumed to be in Tokyo, Japan.

Based on the structural design information, shear models for the buildings considered were created in OpenSees [McKenna et al. 2000]. The structural elements were reduced to a 61-degree-of-freedom system (55 stories above ground and 6 stories underground) and a 14-degree-of-freedom system (13 stories above ground and 1 story underground) with lumped mass, respectively. The stiffness of each story aboveground was represented by a shear spring with a normal trilinear force–deformation hysteresis curve. The shear springs of the underground stories were considered to behave elastically. The internal viscous damping was set equal to 1% and 2% of the critical level at the first natural period for the 55-story building and 13-story buildings, respectively, and their matrices were proportional to the initial stiffness matrices. For the 55-story building, a Maxwell damper model was connected in series on each story level to represent the oil dampers. For both models, springs with negative stiffness were inserted to capture large P-Δ effects in the shear model [Akiyama 2007]. For the current SH model and HH model, the soil amplification factor was not considered and input ground motions were applied at the base of the underground story.

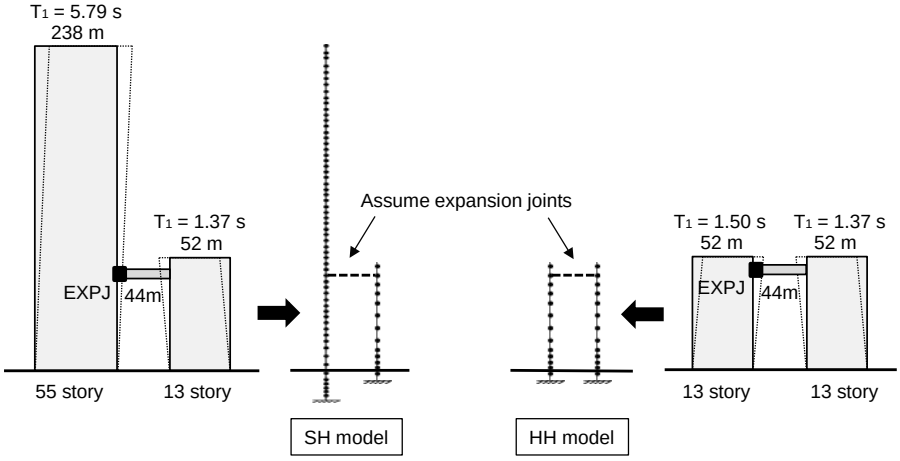

Figure 3 Analytical models of the adjacent buildings at which expansion joints were assumed at a height of 44 m.

5 VULNERABILITY ASSESSMENT OF EXPANSION JOINTS

5.1 Intensity measure

In this section, the vulnerability of expansion joints installed on the adjacent building models is assessed through incremental dynamic analysis (IDA). The appropriate design safety factors for each expansion joint and adjacent building model are determined based on the response database. Under the framework of performance-based earthquake engineering, IDA is often used to quantify the relationship between *EDP* and the intensity measure (*IM*) [Vamvatsikos *et al*. 2002]. For IDA, the appropriate *IM* is essential to reduce the computational cost and variance of response. Commonly used *IM*s are the PGA, PGV, and spectral acceleration at the fundamental period [Biasio *et al*. 2015]. However, in the case of expansion joints where damage depends on the peak relative displacement between two buildings, *IM* should be sensitive to the peak relative displacement. Tubaldi *et al*. [2016] studied the selection of an appropriate *IM* for the seismic pounding problem between two buildings and proposed the following intensity measure, noted by IM_{rel}:

$$IM_{rel} = \gamma_A S_d(T_A)\sqrt{1+R^2-2\rho R},$$

$$R = [\gamma_B S_d(T_B)]/[\gamma_A S_d(T_A)], \text{ and}$$

$$\rho = \frac{8\sqrt{\zeta_A\zeta_B}\left(\zeta_A+\zeta_B\frac{T_A}{T_B}\right)\left(\frac{T_A}{T_B}\right)^{1.5}}{\left[1-\left(\frac{T_A}{T_B}\right)^2\right]^2+4\zeta_A\zeta_B\left[1+\left(\frac{T_A}{T_B}\right)^2\right]\left(\frac{T_A}{T_B}\right)+4\left(\zeta_A{}^2+\zeta_B{}^2\right)\left(\frac{T_A}{T_B}\right)^2}, \quad (5)$$

where $S_d(T)$ denotes the spectral displacement at the fundamental period T of the building and γ denotes the participation factor of the fundamental mode. When computing γ, the modal shape must be normalized to have a unit displacement at the pounding location. Finally, ρ expresses the correlation factor between two buildings with a fundamental period T and damping ratio ζ. In summary, IM_{rel} estimates the peak relative displacement by considering the peak displacements and phase differences of two buildings. The correlation factor ρ is 0.000327 and 0.163 for the SH model and HH model,

respectively. The participation factor at the locations of the expansion joints is 0.228 for the 55-story building and 1.26 for the 13-story building.

5.2 Range of motion of expansion joints

The nominal ranges of motion of the expansion joints for the SH model and HH model are set as listed in Table 5. In Japan, the minimum separation distance is calculated using time history analysis or set as the absolute sum (ABS) of the peak displacements of two buildings from modal response analysis against the Level 2 seismic hazard spectrum [BCJ 2008]. The return period of the Level 2 seismic hazard is approximately 500 years and the Level 2 design acceleration spectrum is presented in Figure 4(a).

In general, the ABS rule gives an overly conservative peak relative displacement, especially when the fundamental periods of two buildings are close [Jeng 1992]. For example, the peak relative displacement estimated by the ABS rule is 395 mm for the SH model and 469 mm for the HH model, whereas the average of the peak relative displacements against ten ground motions fitted to the Level 2 design spectrum from time history analysis was 415 mm for the SH model and 243 mm for the HH model. The ABS rule gives a good estimation for the SH model but a significant overestimation for the HH model. This is because the ABS rule does not consider the phase difference between two buildings, and the effect of the in-phase motions on the peak relative displacement is large for buildings with similar characteristics. The IM_{rel} value for the Japanese Level 2 design spectrum is 365 mm for the SH model and 304 mm for the HH model. In contrast to the ABS rule, the IM_{rel} value gives a good estimation for the HH model. In this study, therefore, the minimum separation distance is set equal to the IM_{rel} value to avoid the overestimation imposed by the ABS rule.

To reduce the number of parameters for comparison reasons, this study fixes the range of motion of the expansion joints to 50% of the clearance, the same as the test specimens. Thus, the safety factor is the only parameter to consider. The safety factors to be considered are 1.2, 1.5, and 1.8, and the corresponding clearance and ranges of motion are obtained as listed in Table 5. The fragility functions defined in the previous section were developed for the expansion joints with the nominal motion range of 175 mm but these fragility functions can be adopted for the expansion joints with different motion ranges as long as their deformation mechanisms are similar to those of the specimens. The authors asked the expansion joint manufacturer to design and fabricate the specimens with the deformation mechanisms exactly same with those for the expansion joints with more common motion ranges (around 500 mm). For dispersion, the expected initial position errors of expansion joints are assumed to be similar for small and large motion ranges. Thus, the dispersion $\beta_{c,i}$ for HP wall DS1-B, SD floor Failure, and SD wall Failure needs to be recalculated, by multiplying 175 mm and dividing by the nominal range of motion presented in Table 5. The dispersions for the other damage states are kept same with those in Table 3 considering a large uncertainty.

Table 5 Clearance and range of motion of expansion joints installed on each model.

Model	IM_{rel} for Japanese Level 2 spectrum (mm) (1)	Safety factor (2)	Clearance between adjacent buildings (mm) = (1)×(2)	Nominal range of motion of expansion joints (mm) = (1)×(2)×0.5
SH model	365	1.2	438	219
		1.5	548	274
		1.8	657	329
HH model	304	1.2	365	183
		1.5	456	228
		1.8	547	274

5.3 Incremental dynamic analysis

For IDA, this study adopts the ‘Far Field’ ground motions provided by FEMA [2009]. Ground motions measured by the instruments with effective periods of less than 6 s were excluded from the original set because the fundamental period of the 55-story building is 5.79 s. From the PEER NGA database [PEER 2017], thirty ground motions (15 record stations × 2 lateral directions) were obtained. Figure 4(a) displays the acceleration response spectra of the thirty ground motions compared with the Japanese Level 2 design spectrum of 2% damping ratio.

The adjacent building models were subjected to the ground motions which were scaled by increasing the index IM_{rel} from 10 to 500 mm with an increment of 10 mm . For each time-history analysis, the peak relative displacement at the location of the expansion joints was recorded and the relationship between IM_{rel} and the peak relative displacement was obtained as shown in Figures 4(b)–(c). There are several notable observations in this figure. First, the reduction of the peak relative displacement can be seen in the range of large IM_{rel} values when the buildings enter the inelastic region. This is because the phase difference of the two buildings responses reduces by the effect of the hysteretic damping that dominates the inelastic range of response [Kasai *et al*. 1996]. Second, the reduction of the peak relative displacement is much larger for

the HH model. It can be assumed that in the HH model two buildings behaved more similarly in the nonlinear range than in the linear range, owing to the period elongation of the original 13-story building after yielding. Third, the dispersion of the peak relative displacement increases once the buildings enter the inelastic range. This can be attributed to the fact that the IM_{rel} value predicts well only the peak relative displacement for elastic systems [Tubaldi *et al*. 2016]. Note that the inelastic behavior of the two buildings does not always reduce the peak relative displacement compared with the elastic system. There is a case in which the peak relative displacement increases with the increase of IM_{rel}. This happens when the two buildings have the same behavior in the elastic range, but different yield displacement and nonlinear behavior, as reported by Tubaldi *et al*. [2015].

Note that, in this IDA, the maximum scaling of the original ground motions was 6.15 for the SH model and 6.73 for the HH model. Considering the different properties of ground motions for different levels of *IM* , a large scaling factor is not appropriate [Baker and Cornell 2005]. As an alternative, Tubaldi *et al*. [2016] conducted cloud analysis instead of IDA to derive the relationship between the peak relative displacement and IM_{rel} by using a set of 240 unscaled ground motions selected by Baker *et al*. [2011]. However, these ground motions were selected in a range of periods up to 5 s, which is shorter than the fundamental period of the 55-story super-high-rise building. Also, the probability of exceedance of the seismic pounding obtained from cloud analysis with bilinear regression and IDA showed a good match, even though a relatively large scaling of the original ground motions was adopted in IDA [Tubaldi *et al*. 2016]. Thus, this alternative was not adopted in the present study.

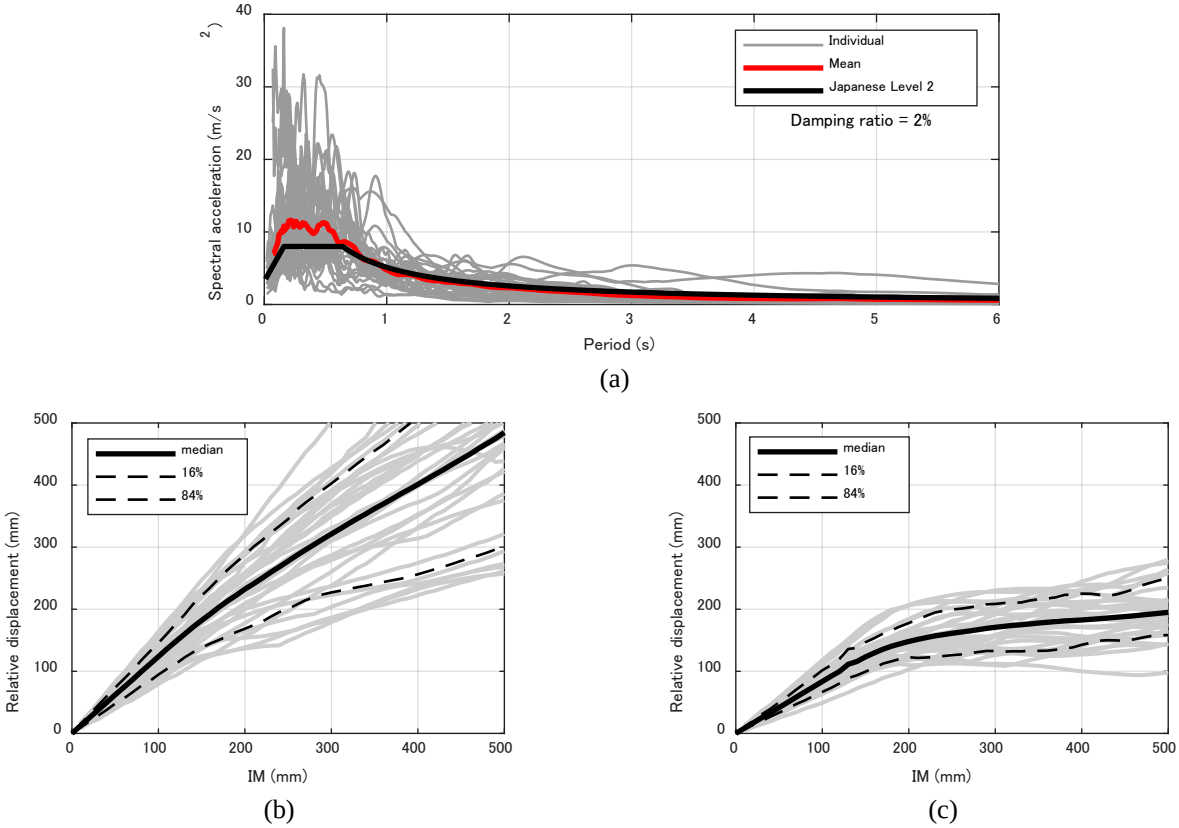

Figure 4 Incremental dynamic analysis: (a) acceleration response spectra of input ground motions and (b) IDA curves for the SH model and (c) for the HH model.

5.4 Vulnerability assessment of HP and SD expansion joints

The probability of a component being in or exceeding a certain damage state $DS = ds_i$ for a given level of a ground motion $IM = im$ can be obtained in a similar manner as Eq. (1):

$$P[DS \geq ds_i \mid IM = im] = \Phi\left(\frac{\ln im - \ln \theta_{DS|IM}}{\beta_{DS|IM}}\right) \tag{6}$$

and the probability of being in $DS = ds_i$ given $IM = im$ is expressed by:

$$P(ds_i \mid im) = \begin{cases} P[DS \geq ds_i \mid im] - P[DS \geq ds_{i+1} \mid im] & 1 \leq i < n \\ P[DS \geq ds_i \mid im] & i = n \end{cases}. \tag{7}$$

For the estimation of $\beta_{DS|IM}$ and $\theta_{DS|IM}$ in Eq. (6), a regression analysis for a sufficient number of *EDP–IM* plots is required, and this can be achieved through IDA. In general, the *EDP–IM* relationship can be approximated by the linear regression in the log–log graph as shown in Figure 5 when systems are in the elastic range. However, when $IM = IM_{rel}$ and *EDP* is the peak relative displacement between two buildings, the linear regression cannot capture the change of the structural responses induced by the structural yielding. Therefore, this study approximates the *EDP–IM* relationship by the bilinear regression in the log–log graph, which is also recommended in Tubaldi *et al*. [2016].

Figure 5(a) demonstrates the parameters of the bilinear regression analysis, where $\ln a_1$ and $\ln a_2$ are the *y*-segments, b_1 and b_2 are the slopes of the lines, and $\ln im^*$ is the breakpoint of the two lines. The parameters of $\ln a_1$, b_1, b_2, and $\ln im^*$ for the approximation of the *EDP–IM* relationship can be estimated using the nonlinear least-square regression. Figure 5(b) shows the bilinear regression curves for the SH model and the HH model using the IDA results. For the SH model, the bilinear curve was approximately linear. This is because the in-phase motion of the two buildings induced by the structural yielding was small. For the HH model, the effect of the yielding was significant, and the bilinear regression provided a good match.

Table 6 lists the parameters to calculate Eq. (6); these were derived by combining the equations from Padgett *et al*. [2008] and Tubaldi *et al*. [2016]. These parameters are obtained from the regression parameters of $\ln a_1$, b_1, b_2, and $\ln im^*$ and have different values before and after the breakpoint im^*. At first, the dispersion of the *EDP* condition upon the *IM*, noted by $\beta_{EDP|IM}$, is obtained using the regression parameters shown in Table 6. The total dispersion $\beta_{DS|IM}$ in Eq. (6) can be obtained using $\beta_{EDP|IM}$, $\beta_{c,i}$ from the developed fragility functions of the expansion joints, and the regression parameters. Finally, $\theta_{DS|IM}$ in Eq. (6) is calculated using the regression parameters and the median capacity of the developed component fragility functions $\theta_{c,i}$. Note that the SD wall expansion joints have two fragility functions corresponding to the DS1 and Failure. These fragility functions produce a negative probability of being in a certain damage state under Eq. (1). Thus, Eq. (1) for DS1 of the SD wall expansion joint was replaced with Eq. (8), as suggested by Porter *et al*. [2007], so that each fragility function does not cross:

$$P[DS \geq ds_1 \mid EDP = edp] = \max\left\{\Phi\left(\frac{\ln edp - \ln \theta_{c,1}}{\beta_{c,1}}\right), \Phi\left(\frac{\ln edp - \ln \theta_{c,2}}{\beta_{c,2}}\right)\right\} . \quad (8)$$

The results of the IDA and the approximated curves from bilinear regression analysis are presented in Figure 6, where the safety factor is set as 1.2. The IDA plots express the mean probability of exceedance for the given $IM_{rel} = im$. Note that the approximation curves are discontinuous at $IM_{rel} = im^* = 230$ mm for the SH model and 140 mm for the HH model, owing to the change of $\theta_{DS|IM}$ and $\beta_{DS|IM}$ before and after the point of im^* [Tubaldi *et al*. 2016]. The left side in Figure 6 shows the results of the SH model, whereas the right side shows the results of the HH model. Each figure contains the IM_{rel} values corresponding to seismic hazard levels of 43-year, 72-year, and 475-year return periods at Tokyo metropolitan area. These hazard levels are often considered in a performance-based design framework [Porter 2003] and the 475-year level is usually set as the target seismic hazard for seismic pounding analysis [CEN 2005, BCJ 2008]. In this study, the target seismic hazard to ensure the safety of the expansion joints is set at the 72-year level. The derivation procedure for these IM_{rel} values is presented in Section 6.

Table 6 Estimation parameters for Eq. (6).

	$IM = im \leq im^*$	$IM = im > im^*$
$\ln edp \mid im$	$\ln a_1 + b_1 \ln im$	$\ln a_1 + (b_1 - b_2)\ln im^* + b_2 \ln im$
$\beta_{EDP\|IM}$	$\sqrt{\frac{\sum_{k=1}^{N_1}(\ln edp_k - (\ln a_1 + b_1 \ln im_k))^2}{N_1 - 2}}$ N_1 = number of simulation cases in $IM = im \leq im^*$	$\sqrt{\frac{\sum_{k=1}^{N_2}(\ln edp_k - (\ln a_1 + (b_1 - b_2)\ln im^* + b_2 \ln im_k))^2}{N_2 - 2}}$ N_2 = number of simulation cases in $IM = im > im^*$
$\beta_{DS\|IM}$	$\frac{\sqrt{\beta_{EDP\|IM}^2 + \beta_{c,i}^2}}{b_1}$	$\frac{\sqrt{\beta_{EDP\|IM}^2 + \beta_{c,i}^2}}{b_2}$
$\ln \theta_{DS\|IM}$	$\frac{\ln \theta_{c,i} - \ln a_1}{b_1}$	$\frac{\ln \theta_{c,i} - (\ln a_1 + (b_1 - b_2)\ln im^*)}{b_2}$

Comparing the SH model and the HH model, it is evident that the expansion joints installed on the HH model have a significantly lower probability of exceedance in the range of $IM_{rel} > im^*$, owing to the nearly-in-phase motions of the two buildings induced by structural yielding. This fact indicates that expansion joints installed on the buildings with close

natural periods that tend to behave similarly in the nonlinear range may suffer from slight damage, and the Failure of those expansion joints is unlikely to occur. For example, against the 72-year seismic hazard level, the SD expansion joints installed on the HH model enter the DS1 with a probability of more than 50%, but the probability for the Failure is only less than 20%. In the case of the HP expansion joints on the HH model, the probability of being in the DS1 is quite low because of their high seismic performance. In summary, the safety factor of 1.2 can be a sufficient value for the HP and SD expansion joints installed on the HH model to ensure their functions against the 72-year hazard level.

The expansion joints installed on the SH model are more vulnerable than those installed on the HH model because the in-phase motions of the two buildings were not observed in a large extend. For the HP expansion joints, the probability of being in DS1 against the 72-year hazard is less than 40% and thus, the safety factor of 1.2 is recommended. This is not the case for the SD expansion joints, owing to their lower seismic capacity compared with the HP expansion joints. For the SD expansion joints, the probability of being in the DS1 against the 72-year hazard exceeds 90%. Especially for the SD wall expansion joints, the probability for Failure exceeds 70% and the safety factor of 1.2 is insufficient to ensure its function. The next section discusses the recommended safety factor to ensure the function of the SD expansion joints installed on the SH model.

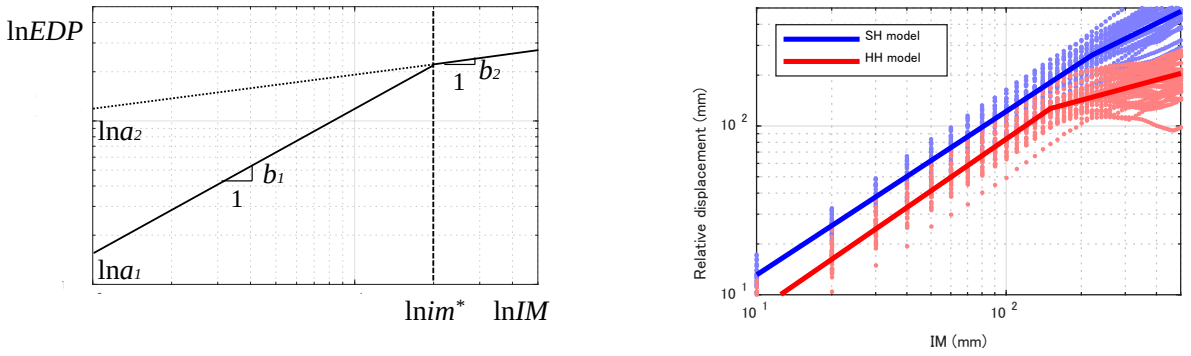

(a) (b)

Figure 5 Bilinear regression analysis: (a) regression parameters and (b) regression curves for IDA results.

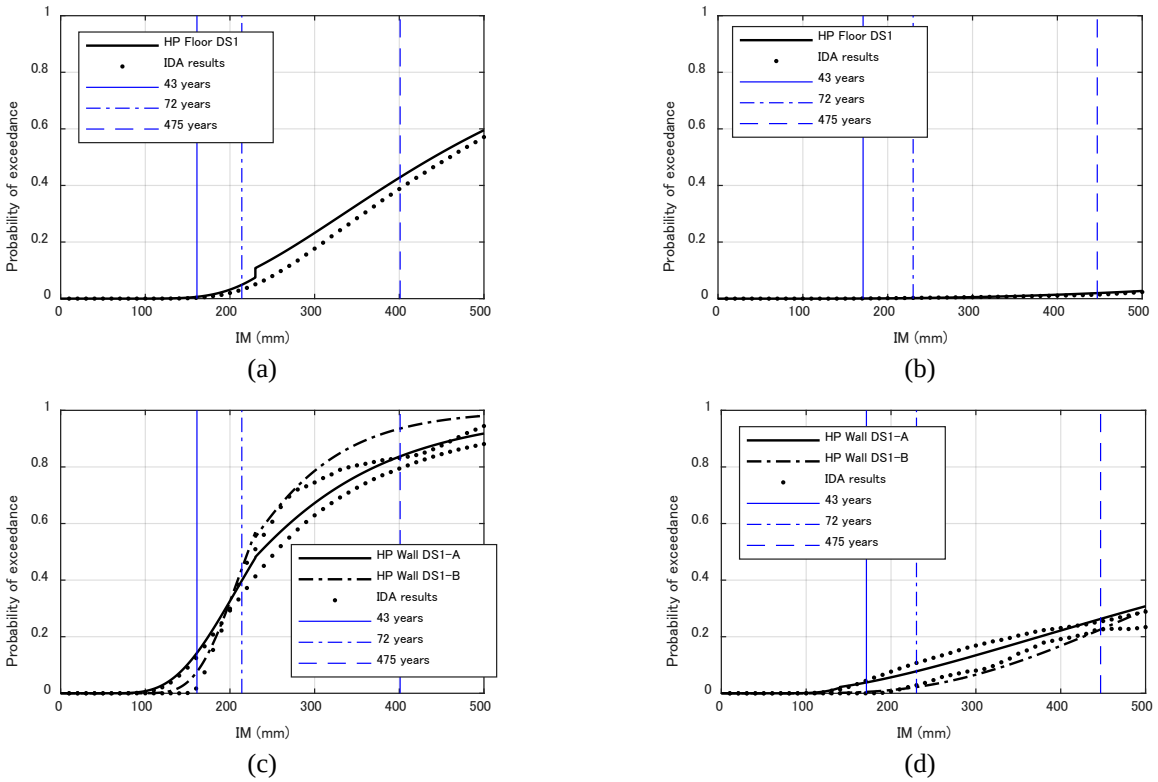

(a) (b) (c) (d)

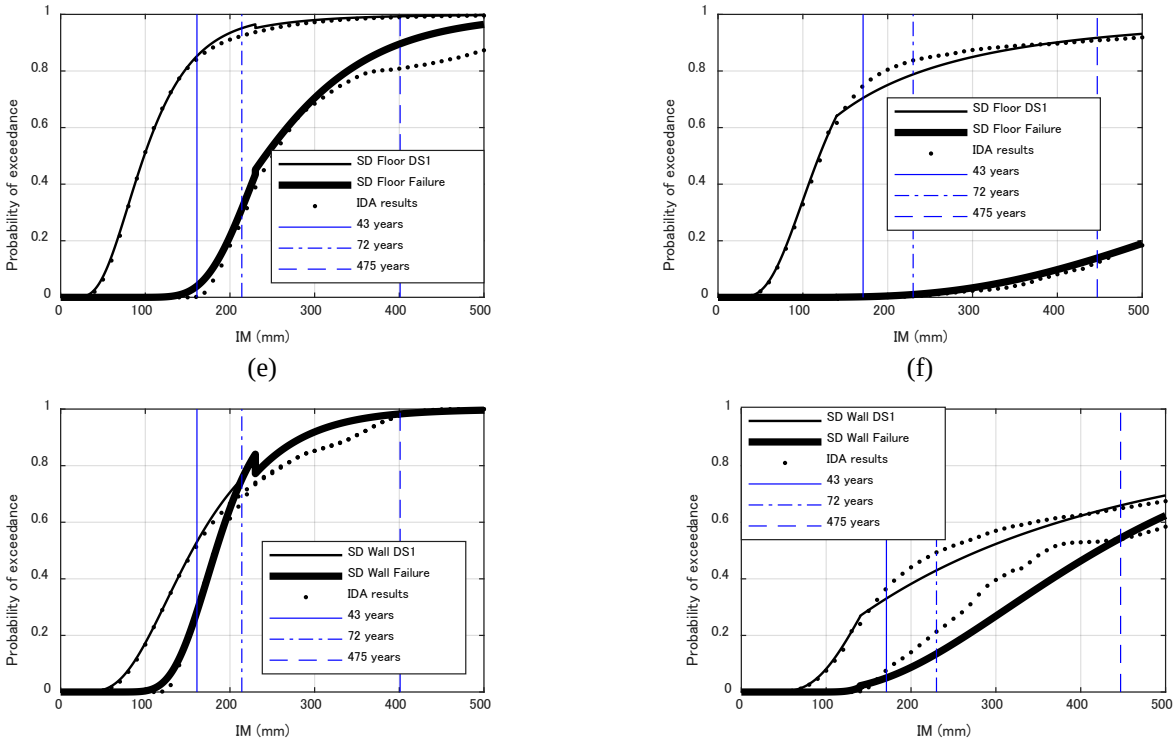

Figure 6 Probability of exceedance of each damage state for a safety factor of 1.2 (left: SH model; right: HH model): (a, b) HP floor DS1, (c, d) HP wall DS1-A and DS1-B, (e, f) SD floor DS1 and Failure, and (g, h) SD wall DS1 and Failure.

5.5 Failure probability of SD expansion joints on the SH model with different safety factors

Figure 7 shows the probabilities of the two failure states, “SD floor Failure” and “SD wall Failure”, for the expansion joints installed on the SH model with safety factors of 1.2, 1.5, and 1.8. Note that “SF” in the figures stands for ‘safety factor’. In general, the increase of the safety factor from 1.2 to 1.5 or from 1.5 to 1.8 results in a 20% decrease of the probability for Failure. For the SD floor expansion joints in Figure 7(a), the recommended safety factor can be set as 1.5 because the failure probability against the 72-year hazard level is less than 10%. For the SD wall expansion joints, however, the safety factor of 1.5 still has a 40% probability for Failure against the 72-year hazard level and the safety factor of 1.8 is recommended.

To summarize this section, it was demonstrated that the building characteristics affect the selection of the performance level and safety factor of expansion joints. For adjacent buildings showing in-phase behavior in the inelastic range, the use of the expansion joints with lower seismic performance, such as the SD expansion joints, can be accepted. In contrast, when the fundamental periods of the two buildings are different, the in-phase motion is not apparent in the inelastic range. In this case, expansion joints with higher seismic performance, such as the HP expansion joints, are recommended. If a large clearance and high safety factor can be used, then the SD expansion joints can be selected.

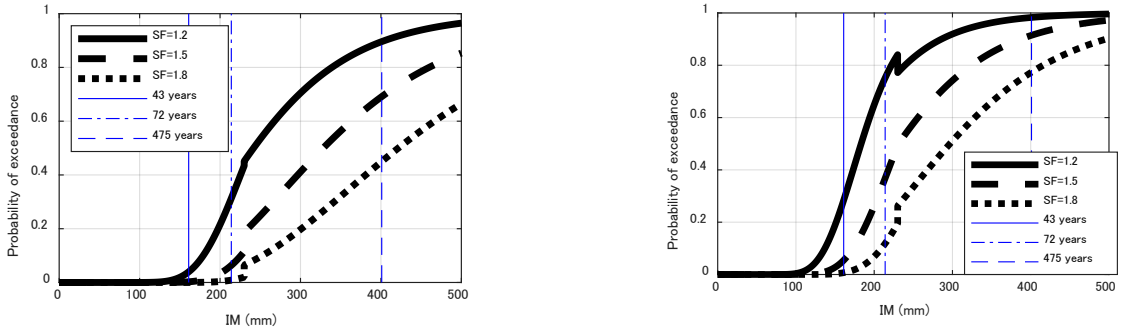

Figure 7 Probability of exceedance for Failure state of SD expansion joints installed on the SH model when safety factors are 1.2, 1.5, and 1.8: (a) SD floor Failure and (b) SD wall Failure.

6 COST-EFFECTIVE SELECTION OF EXPANSION JOINTS

6.1 Concept

Under current design practices, the selection of expansion joints and the associated design of safety factors are not quantitatively determined by structural designers and building owners. Due to the lack of fragility and repair cost information, it is difficult to compare the expected life-cycle costs of various expansion joints under consideration. In contrast to the current situation, building owners want to make an economic selection considering the level of seismic performance, initial cost, expected loss, expected downtime, and so on. Several studies have proposed cost-effective design methods where the optimal design is the one that gives the minimum life-cycle cost [Wen *et al*. 2001, Yanaka *et al*. 2016]. Following this concept, this section demonstrates the procedure for selection of an expansion joint that gives minimum life-cycle cost. Figure 8 illustrates the procedure.

At the first step in Figure 8, the seismic pounding risk analysis of adjacent buildings is performed and the minimum levels of clearance and safety factor are determined. The next step is to select the expansion joints to be installed between adjacent buildings. For each expansion joint under consideration, the fragility function and information on the initial cost and repair cost are obtained. The expected annual loss (EAL) (= expected annual repair cost) of expansion joints is then calculated via the following integrations [Deierlein *et al*. 2003]:

$$EAL = \sum_{i=1}^{n} E(C_R \mid ds_i) \int_{im} P(ds_i \mid im) \mid dv(im) \mid , \tag{9}$$

where $E(C_R|ds_i)$ is the expected repair cost C_R of expansion joints given $DS = ds_i$, obtained from Otsuki *et al*. [2018a], $P(ds_i|im)$ is the probability of being in $DS = ds_i$ given $IM = im$ obtained from Eq. (7), and $v(im)$ is the mean annual frequency of exceedance of $IM = im$. Finally, the expected life-cycle cost $LC(t)$ over the target lifespan of t years is obtained by:

$$LC(t) = EAL \cdot t + C_I \, , \tag{10}$$

where C_I is the initial cost of the expansion joints. The optimal selection of the expansion joints and the safety factor is finally achieved by comparing the calculated life-cycle costs for several expansion joints.

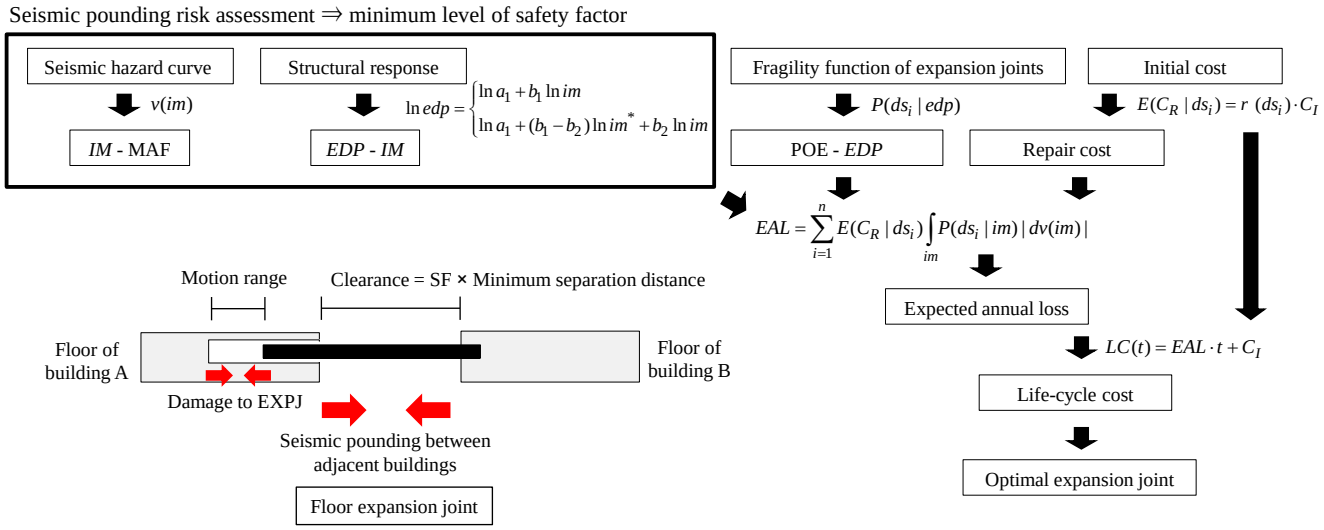

Figure 8 Workflow for cost-effective selection of expansion joints.

6.2 Case study

In this section, case studies are performed to select the cost-effective expansion joint and its safety factor for the adjacent building models. The procedure follows the one described in Figure 8. The available options are the sets of the HP expansion joints or the SD expansion joints. Each set consists of one floor and two wall expansion joints of the tested HP and SD expansion joints. The buildings considered are in Tokyo, and the minimum separation distance between the two buildings is calculated based on the Japanese Level 2 design spectrum. Based on the Section 5, safety factors of 1.2, 1.5, and 1.8 are adopted here and the corresponding nominal ranges of motion are those listed in Table 5. Note that the consequence of Failures is not considered in this study.

6.2.1 Seismic pounding analysis

The likelihood of seismic pounding occurring between adjacent buildings was first evaluated to determine the minimum safety factor. The seismic pounding considered for the SH model and the HH model leads to earthquake-induced collision between the sky bridges and the building surface. Several procedures for probabilistic assessment of seismic pounding were proposed by Tubaldi *et al*. [2012] and Barbato and Tubaldi [2013], but a simple evaluation is conducted here. At first, a seismic hazard curve that expresses $v(im)$ in Eq. (9) for IM_{rel} for the location of the buildings—Tokyo—is created. The Architectural Institute of Japan [AIJ 2016] provides uniform hazard spectra that express spectral accelerations for each period for four different hazard levels (50%, 10%, 5%, and 2% in 50 years) with 5% damping ratio. The corresponding IM_{rel} values of the four hazard levels for each adjacent building model were then calculated using Eq. (5) after the modification of spectral values by $1.5/(1+0.1h)$, where h is the damping ratio of each model. The seismic hazard curves were obtained by performing the hyperbolic approximation described by Bradley *et al*. [2007]. Figure 9(a) shows the obtained seismic hazard curves for the SH model and the HH model. The probability of seismic pounding occurrence given $IM = im$ is then expressed by [Tubaldi *et al*. 2016]:

$$P[u_{rel} \geq \xi \mid IM = im] = \begin{cases} \Phi\left(\dfrac{\ln a_1 + b_1 \ln im - \xi}{\beta_{EDP|IM}}\right) & IM = im \leq im^* \\ \Phi\left(\dfrac{\ln a_1 + (b_1 - b_2)\ln im^* + b_2 \ln im - \xi}{\beta_{EDP|IM}}\right) & IM = im > im^* \end{cases}, \tag{11}$$

where u_{rel} is the peak relative displacement; ξ is the clearance between two buildings as listed in Table 5; and $\ln a_1$, b_1, b_2, $\ln im^*$, and $\beta_{EDP|IM}$ are those values obtained by bilinear regression.

Figures 9(b)–(c) show the probability of seismic pounding with various safety factors obtained using Eq. (11). The target seismic hazard to avoid seismic pounding is set at a 475-year return period (10% in 50 years), which is nearly equivalent to the ones given previously [CEN 2005, BCJ 2008]. For the SH model in Figure 9(b), the consideration of a safety factor of 1.2 is insufficient because seismic pounding occurs with a probability of 40% against the 475-year seismic hazard level. Therefore, it is recommended to have a safety factor of at least 1.5 where the probability of seismic pounding is less than 20% against the 475-year level. In the case of the HH model in Figure 9(c), seismic pounding does not occur even with the minimum level of safety factor = 1.0, which allows the selection of a wide range of expansion joints. In summary, the minimum safety factor of each adjacent building model is determined in consideration of the seismic pounding risk and takes the values of 1.5 for the SH model and 1.0 for the HH model.

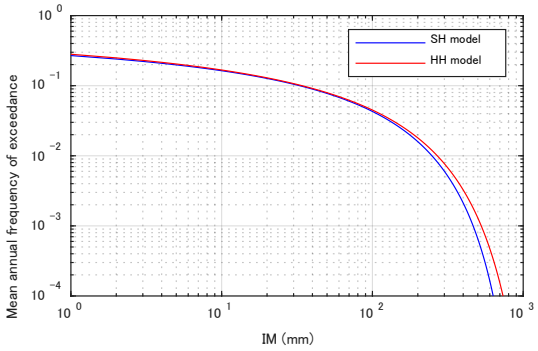

(a)

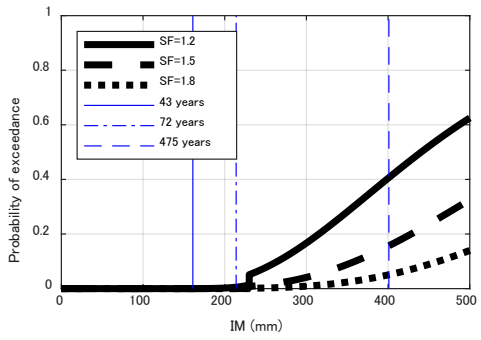

(b)

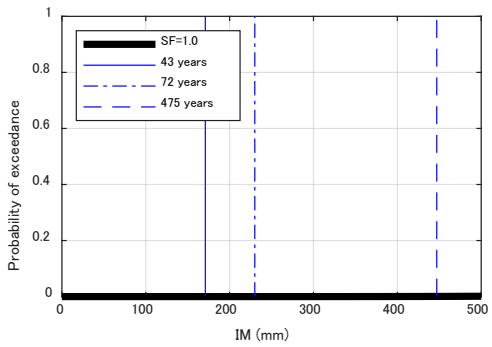

(c)

Figure 9 Seismic pounding risk assessment with various safety factors: (a) seismic hazard curve for IM_{rel} and (b) probability of seismic pounding for the SH model and (c) for the HH model.

6.2.2 *Seismic loss assessment of expansion joints*

The life-cycle cost of building components is usually calculated as the sum of the initial cost, the repair or replacement cost, the cost of injury to people, and the loss of profits due to the loss of building service [Takahashi *et al*. 2004]. However, this analysis does not consider the loss associated with the consequences of injury to people or building service loss because such data is not available. For cost calculation, the inflation rate is ignored and thus the life-cycle cost is defined simply as the sum of the initial cost and the expected loss (or expected repair cost). When further information is obtained in future earthquakes, the loss assessment analysis presented herein should be improved.

The fragility functions used here are those developed in this paper. The initial cost of expansion joints can be divided into the initial material cost, C_M, and the initial construction cost for installation, C_C:

$$C_I = C_M + C_C . \tag{12}$$

It is known that both C_M and C_C increase as the nominal range of motion increases, owing to the increase in the amount of materials used and the complexity in construction. According to the expansion joint manufacturer who joined the authors' shaking table tests, with an increase of the nominal range of motion by 100 mm, the material cost increases approximately by 40% for the tested HP expansion joints and 20% for the tested SD expansion joints. The construction cost increases approximately by 30% for the HP and SD expansion joints. In the experiment, the nominal range of motion of the expansion joints was 175 mm, and the material cost was 695,000 JPY (US$6950) for the set of the HP expansion joints and 405,000 JPY (US$4050) for the set of the SD expansion joints. The construction cost for each set was 300,000 JPY (US$3000). Therefore, in this case study, the following formula is used to estimate the material cost and construction cost for the sets of the HP and SD expansion joints for arbitrary ranges of motion:

$$\begin{aligned} C_{M(HP)} &= 695000\times 1.4^{(D_{exp}-175)/100} \\ C_{M(SD)} &= 405000\times 1.2^{(D_{exp}-175)/100} , \\ C_C &= 300000\times 1.3^{(D_{exp}-175)/100} \end{aligned} \tag{13}$$

where $C_{M(HP)}$ and $C_{M(SD)}$ are the material costs for the sets of HP and SD expansion joints, respectively; C_C is the construction cost for installation; and D_{exp} is the nominal range of motion of the expansion joints in units of millimeters.

Information on the repair cost of the expansion joints is obtained from Otsuki *et al*. [2018a], where the expected repair cost $E(C_R|ds_i)$ for a given damage state $DS = ds_i$ is expressed as the ratio to the initial cost:

$$E(C_R \mid ds_i) = r\ (ds_i)\cdot C_I = r_M(ds_i)\cdot C_M + r_C(ds_i)\cdot C_C , \tag{14}$$

where $r_M(ds_i)$ and $r_C(ds_i)$ are the ratios of repair costs for material and construction to the initial costs for material and construction, respectively.

Using Eq. (9), the EAL of each set of expansion joints is calculated and the results are shown in Figure 10. Comparing between the HP and SD expansion joints, the EAL of the HP expansion joints is significantly smaller than that of the SD expansion joints because of their different seismic capacities. Comparing the SH model with the HH model, the HH model has lower EAL, owing to the in-phase motion of the two buildings in the range of large IM_{rel} values. For all cases, a larger safety factor reduces the EAL. However, the larger safety factor results in the increase of the initial cost. Therefore, the recommended safety factor with the least life-cycle cost is evaluated in the next section.

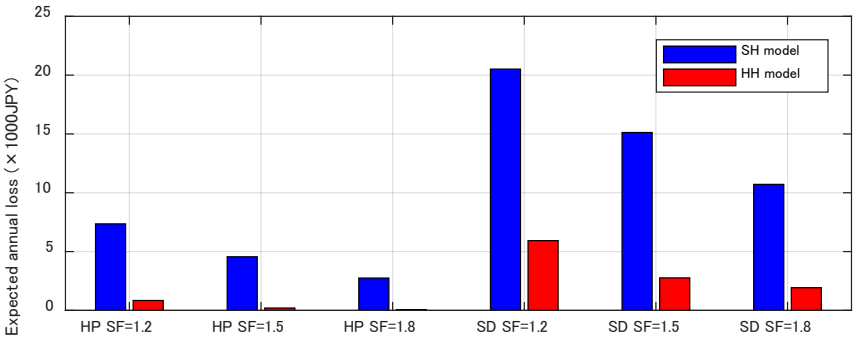

Figure 10 Expected annual loss for each expansion joint and safety factor.

6.2.3 *Comparison of life-cycle cost*

Figure 11 shows the relationship between the lifespan and expected life-cycle cost calculated by Eq. (10). The slope of each line corresponds to the EAL in Figure 10. Here, the optimum expansion joints and safety factors are selected by assuming a 50-year lifespan. For the SH model in Figure 11(a), the optimal selection appears to be the HP expansion joints with safety factor = 1.2 or the SD expansion joints with safety factor = 1.8. However, as mentioned above, a safety factor = 1.2 cannot

be allowed, because of the high possibility of seismic pounding. Therefore, the SD expansion joints with safety factor = 1.8 are selected. For the HH model in Figure 11(b), the optimal selection is the SD expansion joints with safety factor = 1.5 or 1.8. For both cases, an alternative selection can be made depending on the design/construction limitations of the location to be installed or the decision-maker's priorities, such as the lower damage probability for securing the continuation of building service. HP expansion joints appear to be more suitable for this purpose.

The relationship between safety factor and expected life-cycle cost considering the 50-year lifespan is presented in Figure 12. For the SH model in Figure 12(a), the minimum level of the safety factor is 1.5 considering the seismic pounding risk. Thus, the HP expansion joints cannot be the optimal selection and therefore the SD expansion joints with a safety factor of 1.8 are the best choice. For the HH model, the minimum safety factor is taken as 1.0 and the SD expansion joints with a safety factor of 1.5 are the optimal choice. In the case that a large safety factor cannot be taken, owing to the limitations of the installation location, the HP expansion joints with a safety factor of 1.0 can be a suitable alternative.

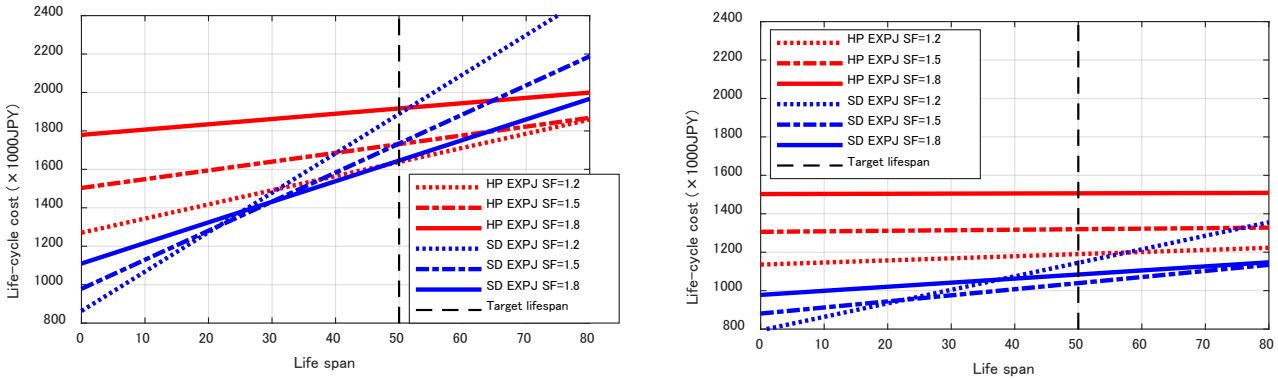

(a) (b)

Figure 11 Sum of the initial cost and expected loss of expansion joints vs lifespan: (a) SH model and (b) HH model.

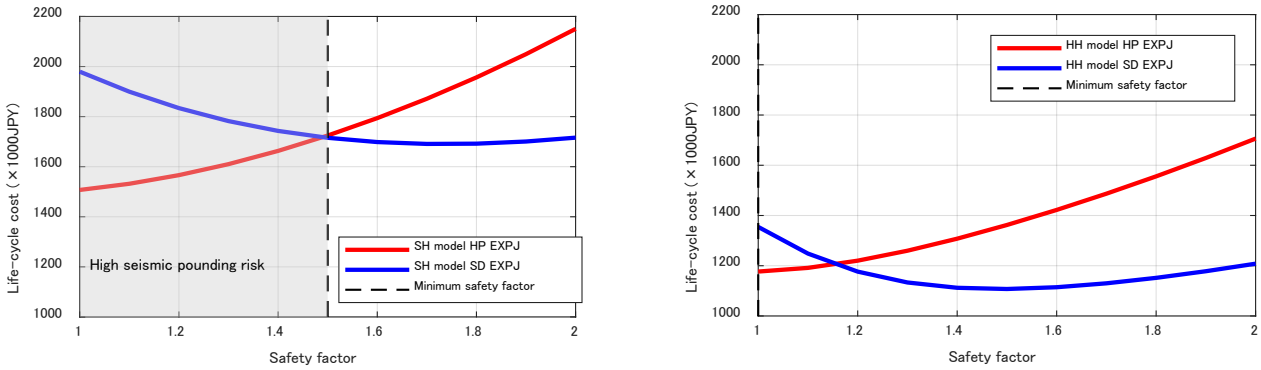

(a) (b)

Figure 12 Summation of the initial cost and expected loss of expansion joints vs safety factor for the 50-year lifespan: (a) SH model and (b) HH model.

7 CONCLUSIONS

This study conducted a vulnerability and seismic loss assessment of expansion joints. Four commonly used expansion joints, high-performance (HP) and standard (SD) expansion joints for floors and walls, were investigated. Their nominal range of motion was 50% of the clearance between adjacent buildings. Two types of adjacent buildings were considered in this study: a 55-story super-high-rise and a 13-story high-rise, denoted by the SH model; and a 13-story high-rise and a 13-story high-rise, denoted by the HH model. First, displacement-dependent fragility functions of the expansion joints were developed based on previous shaking table tests. The vulnerability of the expansion joints installed on the adjacent building models was evaluated through incremental dynamic analysis. In the end, a method for cost-effective selection of expansion joints was presented. Case analytical studies were performed for the considered adjacent building models. The major findings are summarized as follows:

1. Fragility functions for the HP and SD expansion joints for floor and wall were proposed. Because damage to expansion joints mainly depends on the peak relative displacement, the dispersion of the fragility functions was determined in consideration of the initial position errors expected in expansion joints. The median value was taken from the critical length in the drawings and from the experimental results. Considering that the Failures observed to expansion joints

are displacement-dependent, fragility functions of other types of expansion joints are recommended to be constructed from their design drawings by identifying the critical length and the expected initial position errors, as assumed in this paper.

2. The seismic vulnerability assessment in a component-level demonstrated a difference between the performance of HP and SD expansion joints. The probability of the HP expansion joints being in the damage state 1, a minor damage, within the nominal range of motion was less than 20%, whereas it was more than 60% for the SD expansion joints. The probability being in Failure, the loss of functionality, for the SD expansion joints increased rapidly once the predefined nominal range of motion was reached.
3. The building characteristics affect the selection of expansion joints. For adjacent buildings exhibiting in-phase behavior in the inelastic range, such as the HH model, the use of expansion joints with lower seismic performance or a smaller safety factor can be accepted. Thus, for the HH model, a smaller safety factor such as 1.2 can be sufficient to secure the functionality of the HP and SD expansion joints. On the contrary, the in-phase motion of the two buildings was not apparent for the SH model where the difference between the fundamental periods of the two buildings considered is large. This indicates that a safety factor equal or higher than 1.5 is sufficient for the SD expansion joints of the SH model.
4. Compared with the current practice, the benefits of the presented procedure for selection of expansion joints by using their fragility functions are: 1) the decision making is firmly based on quantitative information on the vulnerability and cost of expansion joints, and 2) the alternative selection of expansion joints with different performance levels and safety factors can be made to reach a desired performance level and to consider specific design/construction limitations.
5. Case studies were performed to select the expansion joints for the SH model and the HH model in order to demonstrate the benefits of the proposed procedure. Considering the high seismic pounding risk for the SH model, the optimal selection in terms of life-cycle cost was determined to be the SD expansion joints with a safety factor of 1.8. On the contrary, the probability of occurrence of seismic pounding in the HH model was quite low, and therefore, further options can be available. The optimal selection in this study was the SD expansion joints with a safety factor of 1.5, while the HP expansion joints with a safety factor of 1.0 can be a good alternative in case a higher value for the clearance distance and safety factor for the SD expansion joints cannot be selected.

ACKNOWLEDGMENTS

This work was partially supported by the Tokyo Metropolitan Resilience Project of the National Research Institute for Earth Science and Disaster Resilience (NIED) (subproject C, subject 3 leader: Masahiro Kurata). The authors thank Niitaka Seisakusho Co., Ltd. for providing technical information on expansion joints.

REFERENCES

1. Sullivan TJ., Arifin FA, MacRae GA, Kurata M, Takeda T. “Cost-Effective Consideration of Non-Structural Elements: Lessons from the Canterbury Earthquakes,” 16th European Conference on Earthquake Engineering, June 18-21, 2018.
2. Nakashima M, Nagae T, Enokida R, Kajiwara K. Experiences, accomplishments, lessons, and challenges of E‐defense–Tests using world's largest shaking table. *Japan Architectural Review*. 2018;1:4‐17.
3. Lee T, Kato M, Matsumiya T, Suita K, and Nakashima M. Seismic performance evaluation of non‐structural components: drywall partitions. *Earthquake Engineering & Structural Dynamics.* 2007; 36(3): 367‐382.
4. Anajafi H. and Medina R. Evaluation of ASCE 7 equations for designing acceleration‐sensitive nonstructural components using data from instrumented buildings. *Earthquake Engineering & Structural Dynamics*. 2018;47(4):1075‐1094.
5. Skalomenos KA, Hatzigeorgiou GD, Beskos DE. Modelling level selection for seismic analysis of concrete-filled steel tube/moment resisting frames by using fragility curves. *Earthquake Engineering and Structural Dynamics*. 2015; 44(2): 199-220
6. Sarno L, Magliulo G, D’Angela D, and Cosenza E. Experimental assessment of the seismic performance of hospital cabinets using shake table testing. *Earthquake Engineering & Structural Dynamics*. 2019;48(1): 103–123.
7. Porter, K. Seismic fragility of traction elevators. *Earthquake Engineering & Structural Dynamics.* 2016;45(5): 819–833.
8. Pardalopoulos S. and Pantazopoulou S. Seismic response of nonstructural components attached on multistorey buildings. *Earthquake Engineering & Structural Dynamics*. 2015;44(1): 139–158.
9. Konstantinidis D. and Makris N. Experimental and analytical studies on the response of freestanding laboratory equipment to earthquake shaking. *Earthquake Engineering & Structural Dynamics*. 2009;38(6): 827–848.
10. Porter KA. An overview of PEER’s performance-based earthquake engineering methodology. *Procceedings of the 9th International Conference on Applications of Statics and Probability in Civil Engineering*, San Francisco, CA, 2003.
11. Federal Emergency Management Agency (FEMA). P-58 Next-generation Seismic Performance Assessment for Buildings, Volume 1 – Methodology, FEMA, Washington, D.C., USA, 2012.

12. Architectural Institute of Japan (AIJ), Report on the Damage Investigation of the 2005 West off Fukuoka Earthquake, Tokyo, 2005. (in Japanese)
13. National Institute for Land and Infrastructure Management (NILIM)and Building Research Institute (BRI). Quick Report of the Field Survey on the Building Damage by the 2016 Kumamoto Earthquake. Technical Note of NILIM No. 929 and Building Research Data No. 173, Tokyo, JAPAN, 2016. (in Japanese)
14. Kasai K, Mita A, Kitamura H, Matsuda K, Morgan T, Taylor A. Performance of Seismic Protection Technologies during the 2011 Tohoku-Oki Earthquake. *Earthquake Spectra*. 2013; 29(1): 265-293.
15. Bertero V V. Observations of structural pounding. Proceedings of the International Conference on the Mexico Earthquake 1985: Factors Involved and Lessons Learned; September 19-21, 1986; Mexico City, Mexico.
16. Filiatrault A, Cervantes M, Folz B, Prion H. Pounding of buildings during earthquakes: a Canadian perspective. Canadian Journal of Civil Engineering. 1994; 21(2): 251-265.
17. Kasai K, Maison B F. Building Pounding Damage During the 1989 Loma Prieta Earthquake. *Engineering Structures*. 1997; 19(3): 195-207.
18. Public Works Research Institute (PWRI), Report on the disaster caused by the 1995 Hyogoken Nanbu Earthquake. *Journal of Research*. 1997; 33.
19. Cole L G, Dhakal P R, Turner M F. Building pounding damage observed in the 2011 Christchurch earthquake. Earthquake Engng Struc Dyn. 2012; 41: 893-913.
20. Architectural Institute of Japan, Tohoku branch (AIJ), Report on the disaster caused by the 2011 Tohoku Earthquake. 2013. (in Japanese)
21. Isobe D, Yamashita T, Tagawa H, Kaneko M, Takahashi T, Motoyui S. Motion analysis of furniture under seismic excitation using the finite element method. *Japan Architectural Review*. 2018;1:44‐55.
22. Japanese Society of Seismic Isolation (JSSI). Guideline on Expansion Joints for Seismic Isolation buildings. JSSI, Tokyo, JAPAN, 2013. (in Japanese)
23. Japan Expansion Joint Association (JEJA). Guideline of Expansion Joints for Buildings. JEJA, Tokyo, JAPAN, 2016. (in Japanese)
24. Building Center of Japan (BCJ). Criteria for Structural Calculation for Buildings Split by Expansion Joints, Building letter, 2008; 506. (in Japanese)
25. International Conference of Building Officials (ICBO). Uniform Building Code. ICBO, Whittier, CA, USA, 1997.
26. European Committee for Standardization (CEN). *European Standard EN 1998-1: 2005 Eurocode 8: Design of structures for earthquake resistance. Part 1: General rules, Seismic action and rules for buildings*. European Committee for Standardization: Brussels, Belgium, 2005.
27. Construction and Planning Administration Ministry of Interior. *Seismic Provisions*. Building Code (TBC): Taipei, Taiwan, 1997.
28. Tubaldi E, Freddi F, Barbato M. Probabilistic seismic demand model for pounding risk assessment. *Earthquake Engineering & Structural Dynamics.* 2016; 45(11): 1743–1758.
29. Architectural Institute of Japan (AIJ). Recommendation for Aseismic Design and Construction of Nostructural Elements. AIJ, Tokyo, 2003. (in Japanese)
30. Otsuki Y, Kurata M, Skalomenos K, Ikeda Y. Damage sequence and safety margin assessment of expansion joints by shake table testing. 2018a. (under the revision)
31. Porter K, Kennedy R, Bachman R. Creating Fragility Functions for Performance-Based Earthquake Engineering. *Earthquake Spectra*. 2007; 23(2): 471–489.
32. Japanese Society of Seismic Isolation (JSSI). Maintenance and Management Standards for Isolation Building. JSSI, Tokyo, 2010. (in Japanese)
33. Kasai K, Jagiasi A, Jeng V. Inelastic vibration phase theory for seismic pounding mitigation. *Journal of Structural Engineering*. 1996; 122(10): 1133-1146.
34. Tubaldi E, Barbato M. Probabilistic risk analysis of structural impact in seismic events for linear and nonlinear systems. *Earthquake Engineering & Structural Dynamics*. 2015; 44(3): 491–493.
35. Otsuki Y, Buyco K, Kurata M, Speicher M. Feasibility Study on Multi-code Seismic Evaluation of a Landmark Building. Proceedings of the 11th National Conference in Earthquake Engineering, Earthquake Engineering Research Institute, Los Angeles, CA. 2018b.
36. Lin J, Weng C. Probability analysis of seismic pounding of adjacent buildings. *Earthquake Engineering & Structural Dynamics*. 2001; 30(10): 1539–1557.
37. McKenna F, Fenves GL, Scott MH. Open system for earthquake engineering simulation. University of California, Berkeley, CA. 2000.
38. Akiyama H. P-δ Effect in Earthquake Resistant Design for Shear Type Multi-story Frames. *Journal of Structure and Construction Engineering*. 2007; 617: 87-94. (in Japanese)
39. Vamvatsikos D, Cornell A. Incremental dynamic analysis. *Earthquake Engineering & Structural Dynamics*. 2002; 31(3): 491–514.

40. Biasio M, Grange S, Dufour F, Allain F, Petre-Lazar I. Intensity measures for probabilistic assessment of non-structural components acceleration demand. *Earthquake Engineering & Structural Dynamics*. 2015; 44(13): 2261–2280.
41. Jeng V, Kasai K, Maison BF. A spectral difference method to estimate building separations to avoid pounding. *Earthquake Spectra*. 1992; 8(2):201–223.
42. Federal Emergency Management Agency (FEMA). P-695 Quantification of Building Seismic Performance Factors, FEMA, Washington, D.C., 2009.
43. Pacific Earthquake Engineering Research Center (PEER). Strong Motions Database, University of California, Berkeley, available at http://ngawest2.berkeley.edu/ [last access February 2017].
44. Baker JW, Cornell, CA, 2005. Vector-Valued Ground Motion Intensity Measures for Probabilistic Seismic Demand Analysis, Report No. 150, John A. Blume Earthquake Engineering Center, Stanford, CA, 321 pp.
45. Baker JW, Jayaram N, Shahi S. Ground motion studies for transportation systems, 2011. available at http://peer.berkeley.edu/transportation/projects/ground-motion-studies-for-transportation-systems/ [last access February 2017].
46. Padgett J, Nielson B, DesRoches R. Selection of optimal intensity measures in probabilistic seismic demand models of highway bridge portfolios. *Earthquake Engineering & Structural Dynamics*. 2008; 37(5).
47. Wen YK, Kang YJ. Minimum building life-cycle cost design criteria. II: Applications. 2001. *Journal of Structural Engineering*. 2001; 127(3): 338-346.
48. Yanaka M, Ghasemi S, Nowak A. Reliability-based and life-cycle cost-oriented design recommendations for prestressed concrete bridge girders. *Structural Concrete*. 2016; 17(5): 836–847.
49. Deierlein GG, Krawinkler H, Cornell CA. A framework for performance-based earthquake engineering. Proceedings of the 2003 Pacific Conference on Earthquake Engineering.
50. Tubaldi E, Barbato M, Ghazizadeh S. A probabilistic performance-based risk assessment approach for seismic pounding with efficient application to linear systems. *Structural Safety*. 2012; 36: 14–22.
51. Barbato M, Tubaldi E. A probabilistic performance-based approach for mitigating the seismic pounding risk between adjacent buildings. *Earthquake Engineering & Structural Dynamics*. 2013; 42(8): 1203–1219.
52. Architectural Institute of Japan (AIJ). Guidebook of Recommendations for Loads on Buildings, Maruzen. 2016. (in Japanese)
53. Bradley B, Dhakal R, Cubrinovski M, Mander J, MacRae G. Improved seismic hazard model with application to probabilistic seismic demand analysis. *Earthquake Engineering & Structural Dynamics*. 2007; 36(14): 2211–2225.
54. Takahashi Y, Kiureghian A, Ang A. Life-cycle cost analysis based on a renewal model of earthquake occurrences. *Earthquake Engineering & Structural Dynamics*. 2004; 33(7): 859–880.